Article

Dynamic Characteristics of Reconstituted Silt Influenced by Axial Unloading Intensity and Fine Particle Content

Fanli Meng [1], Changqing Xia [2,3,4,*], Min Zhu [2,3,4], Zhijun Tong [1] and Chengyuan Lu [1]

[1] College of Civil Engineering, Zhejiang University of Technology, Hangzhou 310023, China; zgdmfl@zjut.edu.cn (F.M.); zgdtzj@163.com (Z.T.); zgdlucy@sina.com (C.L.)

[2] College of Civil and Transportation Engineering, Shenzhen University, Shenzhen 518061, China; zhuminfnf@szu.edu.cn

[3] Underground Polis Academy, Shenzhen University, Shenzhen 518061, China

[4] Key Laboratory of Coastal Urban Resilient Infrastructures (MOE), Shenzhen University, Shenzhen 518061, China

[*] Correspondence: xiacq09@szu.edu.cn

Abstract: The stress disturbance induced by adjacent construction has a significant impact on the dynamic characteristics of the soil, resulting in complex long-term tunnel settlement under train vibration load. Through a series of dynamic triaxial tests, the effects of different fine particle contents and axial unloading intensities on the permanent axial deformation and excess pore water pressure of reconstituted silt under long-term cyclic loading were investigated. The findings show that as fine particle content in the silt increases, the threshold dynamic stress and failure cycle number decrease at first, then increase, reaching a minimum value at 10% fine particle content. The dynamic characteristics of silt are significantly affected by axial unloading, and the dynamic stress threshold amplitude of a soil sample decreases as the unloading strength increases. The accumulation of silt deformation caused by long-term cyclic load can be effectively controlled by ensuring drainage conditions.

Keywords: reconstituted silt; cyclic loading; fine particle content; axial unloading intensity; permanent axial strain; excess pore water pressure

1. Introduction

The permanent settlement caused by the cyclic loading of metro trains has greatly increased the operation risk and maintenance cost of urban metro tunnels [1,2]. On the southeast coast of China, many metro lines cross the silt stratum with rich groundwater and complex geological conditions. In particular, the construction activities above the existing metro tunnels are increasing year by year due to the rapid development of the city [3]. Under the coupling effect of the above foundation pit excavation and the train vibration, the deformation and liquefaction of the silt surrounding existing shield tunnels must be studied.

Currently a large number of laboratory tests [4–7] and field tests [8] on the dynamic characteristics of silt under cyclic loading have been conducted. Georgiannou et al. (1991) pointed out that there is a threshold strain that determines the stable and unstable patterns of the clayey sand under undrained cyclic triaxial loading [9]. In some other research, the threshold stress has been used. When the dynamic stress amplitude exceeds the value, the plastic deformation and excess pore water pressure of the soil increase significantly as the number of cycles increases. When the dynamic stress amplitude is less than the threshold value, the plastic deformation and excess pore water pressure of soil are relatively small [10,11]. Rapid increase in the excess pore water pressure may cause soil liquefaction [12]. In particular, current research focuses on the influence of fine particles on the liquefaction resistance of soil during earthquakes. Dash et al. (2010) investigated the influence of fine particles on the dynamic properties of silty sand under cyclic loading. The

test results reveal that the non-plastic fines have a significant impact on the cyclic resistance ratio (CRR) and pore water pressure accumulation [13]. Akhila et al. (2019) studied the effect of clay content and gradation on the liquefaction resistance of sand–clay mixtures through triaxial cyclic tests, and discovered that the liquefaction resistance decreased with the increase of clay content [14]. Ghani et al. (2021) systematically summarized the effects of fine particle content and plasticity index on liquefaction resistance of soil [15]. At the same time, the effect of principal stress rotation induced by dynamic stress paths on the deformation and stability of soils has been further studied [16,17]. As the problem of mud pumping (subgrade fluidization and fines migration into the ballast voids) in high-speed railways becomes more prevalent, research into the effect of fine particle content on the dynamic response of high-speed railway subgrades under a train load is gradually increasing. Indraratna et al. (2020) studied the cyclic load response of a high-speed railway subgrade with different kaolin contents [18]. The findings show that increasing the content of fine particles reduces the static undrained shear strength of soil mass, improves the plasticity index, and the fluidization resistance of the soil sample. However, considering that mud pumping occurs primarily on the soil surface, the confining pressure of the soil is limited to 20 kPa. Few studies on the development of permanent strain and pore water pressure of surrounding silt under long-term metro cyclic load have been carried out. It is particularly unclear how the fine particle content affects the dynamic characteristics of silt.

The change in soil stress state caused by adjacent construction is an important reason for the deformation of the stratum and the existing shield tunnel [19,20], which also has an impact on the cyclic deformation characteristics of the soil in the influenced zones. Therefore, the influence of surrounding disturbance should be considered when analyzing the dynamic characteristics of the soil around the tunnel under cyclic loading. However, in most of the dynamic load tests, the confining pressure and static deviator stress are maintained at a constant level throughout the cyclic loading process, and the impact of stress disturbance caused by adjacent construction is not taken into account. The effect of stress disturbance on soil deformation under long-term cyclic loading has only been considered in a few studies. Liu et al. (2021) studied the influence of lateral unloading between cycles on the deformation of kaolin clay, and the results showed that the accumulated axial strain increased significantly with the increase in lateral unloading [21]. Liu et al. (2021) investigated the effect of axial and lateral stress disturbances on the undrained dynamic response characteristics of kaolin clay. The results showed that the accumulated axial strain is controlled by the static deviator stress ratio (q/p_0) and is independent of the stress disturbance schemes [22]. The related research is mainly focused on kaolin clay, and the effect of stress disturbance on permanent strain and pore water pressure of silt under cyclic loading needs to be further investigated.

In this paper, a series of undrained cyclic triaxial tests of silt with varying fine particle content and stress disturbance are presented. The static axial stress of the soil samples is reduced by various magnitudes to simulate the impact of foundation pit excavation and structural construction above the tunnel. By analyzing the accumulated axial strain and excess pore water pressure (EPWP) of the soil samples under long-term cyclic loading, the influence of fine particle content and axial unloading strength on the dynamic response of silt is discussed. The findings of the study can be used to develop a theoretical framework for assessing the long-term deformation of the existing tunnel due to the combined effects of adjacent construction and train loads.

2. Test Program

2.1. Soil

The silt was obtained from the saturated silt layer at a depth of 12–15 m in the Xiasha section of the Hangzhou Metro Line 1. As the laboratory tests using undisturbed soil samples are affected by many factors including sampling disturbance, spatial variability of soil parameters, and the difficulty in controlling the content of fine particles, the soil

samples of reconstituted silt were used instead. The basic physical indexes of in-situ silt measured through geotechnical tests are summarized in Table 1.

Table 1. Physical properties of the silt.

$w/\%$	$\rho_d/\text{g/cm}^3$	$\rho/\text{g/cm}^3$	G_s	e	$w_L/\%$	$w_P/\%$	I_P
28.91	1.49	1.94	2.69	0.79	31.3	24.70	6.74

Note: w = water content; ρ_d = dry density; ρ = natural density; G_s = specific gravity; e = void ratio; w_L = liquid limit; w_P = plastic limit; I_P = plastic index.

Kaolin clay was chosen as the mixture soil in order to obtain silt with varying fine particle content. Table 2 shows the particle size distribution of silt and kaolin clay as determined by sieve analysis. Five groups of soil with clay content of 7%, 8%, 10%, 12%, and 14% were calculated based on the particle size distribution.

Table 2. Particle size distribution of soil.

Particle Size	Silt	Kaolin Clay
Fine sand (0.25–0.075 mm) (%)	2.48	0
Silt (0.075–0.005 mm) (%)	90.54	49.80
Clay (<0.005 mm) (%)	6.98	50.20

2.2. Parameters of the Cyclic Loading

1. Wave form and frequency of the cyclic loading

It is critical to determine the reasonable wave form of cyclic loading. Tang et al. (2008) discovered that the wave form of the dynamic stress in the surrounding soil has obvious harmonic characteristics based on measurements taken along the Shanghai Metro Line. The frequency of cyclic loading was divided into two types, 2.4–2.6 Hz and 0.4–0.6 Hz, due to the different intervals between adjacent train wheels [1]. Based on a large number of tests, Ding et al. (2015) concluded that sine waves can be used to represent a variety of dynamic loading in situ in laboratory tests, including traffic load, seismic load, and wave load [23]. The peak displacement of the soil surrounding the metro tunnel induced by the train vibration load, according to Gong et al. (2005), occurs near 1 Hz and 3 Hz (especially near 1 Hz) [24]. As a result, the cyclic loading in the test is determined to be a sine wave with a frequency of 1 Hz.

2. Amplitude of the cyclic loading

From the field measurements of the Guangzhou-Shenzhen railway and the Beijing circular railway, an empirical formula was made to predict the dynamic stress amplitude on the railroad subgrade surface [4]:

$$\sigma_d = 0.26P(1 + 0.004V) \tag{1}$$

where σ_d is the dynamic vertical stress amplitude; P is the axle load of the train; and V is the train speed. The parameters of 0.26 and 0.004 are the axle load coefficient and speed coefficient, respectively. The axle load of Hangzhou Metro Line is 8 t under no load and 14 t under full load, with a train speed of 15 km/h to 80 km/h. The dynamic stress amplitude range of the soil can be calculated to be 22–48 kPa.

3. The number of cycles and the failure criterion

The number of cycles is set at 10,000. Liquefaction and strain failure criteria are currently the most common failure criteria for soil cyclic tests. The failure standard for liquefaction in sand is "initial liquefaction" ($u_d = \sigma_3$, where u_d is the dynamic pore water pressure, σ_3 is the confining pressure) [25], but the relatively low permeability of silt causes

a delay in the pore water pressure measurement. As a result, the strain failure criterion is used, with the permanent axial strain set to 5%.

2.3. Unloading and Reloading Stress Paths

The sample's confining pressure is set to 100 kPa, and the consolidation ratio K_c (axial pressure/confining pressure in the consolidation stage) is set to 1.0. The total unloading capacity is set at 40 kPa to simulate the construction of a shallow foundation pit with an excavation depth of less than 5 m above the existing tunnel. Unloading intensities of 10 kPa, 20 kPa, and 40 kPa were used to simulate the staged excavation of the foundation pit. Table 3 contains the test scheme. Groups AU and AD are the undrained and drained cyclic tests of silt with different fine particle contents. The undrained cyclic tests after the axial unloading stress paths, which take into account the staged excavation of the above foundation pit, are referred to as Group BU. The undrained cyclic tests after axial unloading and the reloading stress path, which consider the construction of the main structure after excavation, are referred to as Group CU. In each group, different dynamic stress was applied on the sample until the threshold dynamic stress amplitude was found. The static shear properties of the soil under unloading and reloading stress paths can be seen in reference [3].

Table 3. Test scheme.

Number	Fine Particle Content/%	Effective Axial Stress Paths/kPa	Drainage Conditions (Cyclic Tests)
AU/AD-1	7	100	Undrained/Drained
AU/AD-1	8	100	Undrained/Drained
AU/AD-1	10	100	Undrained/Drained
AU/AD-1	12	100	Undrained/Drained
AU/AD-1	14	100	Undrained/Drained
BU-1	8	100→90→80→70→60	Undrained
BU-2	8	100→80→60	Undrained
BU-3	8	100→60	Undrained
CU-1	8	100→90→80→70→60→100	Undrained
CU-2	8	100→80→60→100	Undrained
CU-3	8	100→60→100	Undrained

2.4. Test Procedures

As shown in Figure 1, the cyclic tests were carried out using the TYD-20 dynamic triaxial test apparatus, which can apply dynamic load with various waveforms and measure real-time data including dynamic stress, dynamic strain, and dynamic pore water pressure of the soil samples under long-term cyclic loading. The following is a list of detailed test procedures.

Figure 1. TYD-20 dynamic triaxial test apparatus.

1. Sample preparation

    The required weight of the silt and kaolin clay was calculated based on the parameters of the soil samples, including a dry density of 1.497 g/cm^3, diameter of 39.1 mm, height of 79.8 mm, and fine particle content. However, the soil sample with 28.91% water content liquefies easily in the compaction process. The compaction curve was obtained, and the optimum water content and maximum dry density were 26% and 1.523 g/cm^3, respectively. The dry density of the reconstituted silt under 22% water content was 1.497 g/cm^3, which is close to the dry density of in-situ silt. As a result, the de-aired water was added based on the controlled water content of 22%. The compaction method was chosen in accordance with the Specification of Soil Test (GB/T50123-2019) to ensure the uniformity of the soil sample. The soil samples were compacted into five layers, and the interface between adjacent layers was scraped to ensure good contact.

2. Saturation

    The soil sample was placed in the vacuum pumping cylinder and saturated using the vacuum saturation method. The negative pressure was maintained at 100 kPa, and de-aired water was slowly injected from the bottom of the soil sample. After the sample was completely submerged in water, draining was stopped, and air extraction was continued for another half hour. The valves were then closed completely.

3. Consolidation

    To ensure isotropic consolidation, the confining pressure was set at 100 kPa and the axial force was set at 120 N. The soil sample was installed in the pressure chamber, and then water was injected and pore water pressure was zeroed. The confining pressure was added, and the consolidation was started after the pore water pressure had stabilized and the check saturation had reached the specified value. The original height and maximum pore water pressure were recorded, and then the drainage valve was kept open until the pore water pressure had dropped by more than 95%.

4. Unloading and reloading

    The total axial stress of the soil sample was unloaded in multiple stages according to the test scheme after initial consolidation. In the reloading stress path, the axial stress was increased to its initial value. All unloading and reloading rates were set to 1 kPa/min. The drainage valve was continuously open and the sample was allowed to be completely consolidated after each stage of unloading and reloading.

5. Cyclic loading

    The stress amplitude, number of cycles, data acquisition time interval, and termination conditions were all set at the start of the cyclic loading process. For the drained tests, the drainage valve was kept open, and for the undrained tests, it was closed. The pore pressure, accumulated strain, and other data were automatically recorded during the test, and the tests were terminated once the failure standard was met.

3. Dynamic Response of the Silt Containing Fine Particles under Conventional Triaxial Stress Path

3.1. Undrained Cyclic Tests

The development of permanent axial strain versus number of cycles was obtained through long-term cyclic tests on silt with different fine particle contents, as shown in Figure 2a–e. Although the failure axial strain was 5%, the upper limit of the strain in the figures was set to 2% to show the strain development of all loading cycles clearly. The permanent axial strain curve can be divided into stable and failure modes based on different dynamic stress amplitudes. The permanent axial strain of the stable mode increases rapidly in the first few cycles, indicating that the soil sample is significantly compacted. The growth rate of the accumulated strain gradually decreases as the number of cycles increases, and the strain tends to a stable value, indicating that the specimen exhibits an elastic response.

In the early stages of cyclic loading, the permanent axial strain of the failure mode is nearly identical to that of the stable mode. The structure of the soil samples is damaged when a certain number of cycles is reached, and the strain increases dramatically in a short period of time. The permanent axial strain curves change from stable to failure mode as dynamic stress amplitude increases, with the threshold stress amplitude serving as the demarcation point. The number of vibration cycles required to reach the failure strain decreases significantly as the dynamic stress amplitude exceeds the threshold value.
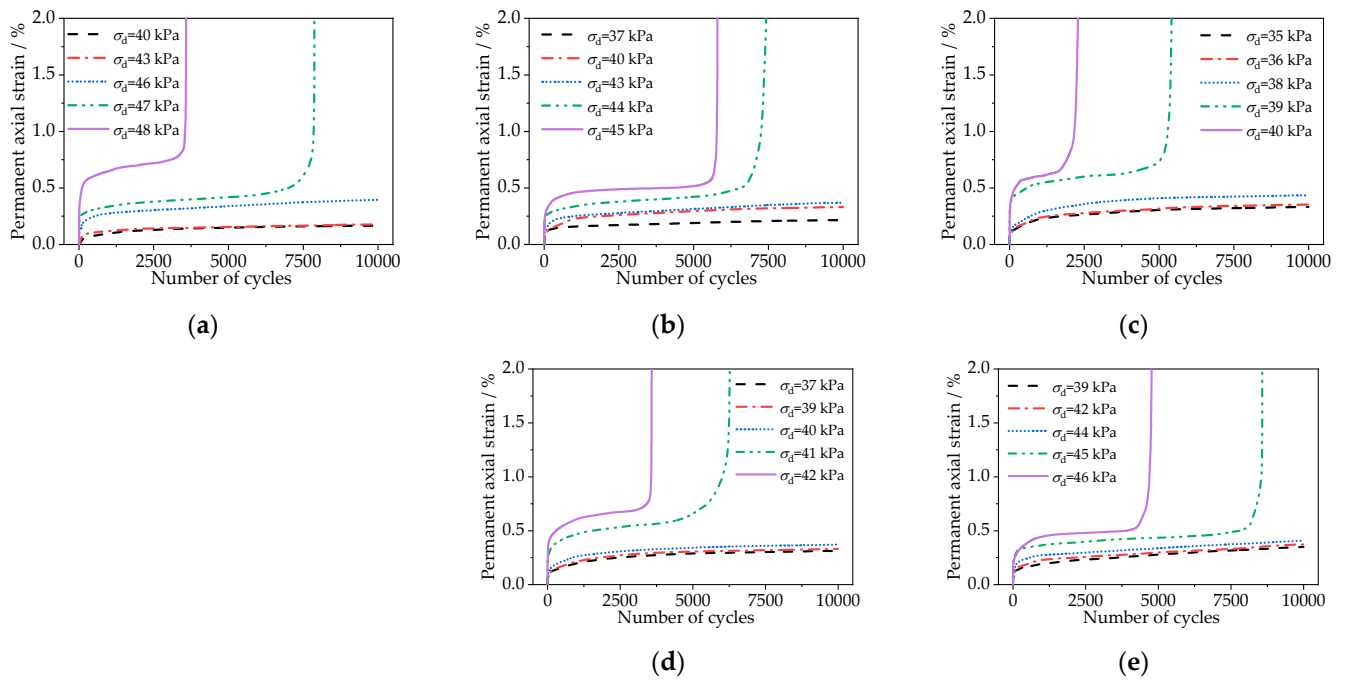
Figure 2. Permanent axial strain of the saturated silt with different fine particle contents under undrained conditions. (**a**) 7% fine particle content; (**b**) 8% fine particle content; (**c**) 10% fine particle content; (**d**) 12% fine particle content; (**e**) 14% fine particle content.

Figure 3a,b are the stress paths at σ_d = 40 kPa (stable mode) and σ_d = 48 kPa (failure mode) with the fine particle content of 7%. With the increase in the number of cycles, p' and q remain almost unchanged when σ_d = 40 kPa. When σ_d = 48 kPa, p' continues to decrease and q remains stable at the initial stage. As the number of cycles approaches the critical value, the excess pore water pressure accumulates rapidly, and the sample has difficulty bearing the cyclic dynamic stress. The lower limit of q increases and the upper limit decreases, and the soil sample reaches failure condition. Figure 4 shows the accumulative axial strain development under stable and destructive modes, and the permanent axial strain is the lower envelope of accumulative axial strain.
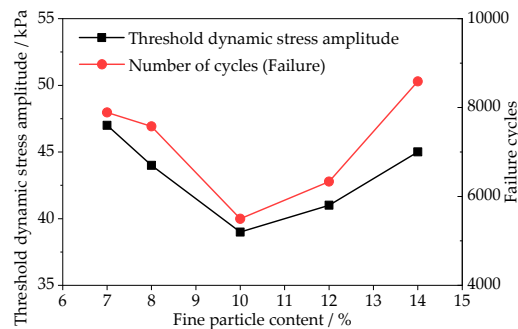
Figure 5 shows the influence of different fine particle contents on the threshold dynamic stress amplitude and failure cycles at 5% axial strain. The threshold dynamic stress amplitude and failure cycles both decrease at first, then increase. At 10% fine particle content, the stress amplitude and number of cycles reach a minimum of 39 kPa and 5495, respectively, indicating that the silt is more vulnerable to long-term traffic load. When the fine particle content is less than 10%, the fine particles act as a lubricant and allow the coarse particles to slide, which causes the threshold dynamic stress amplitude to decrease. When fine particle content exceeds 10%, its viscous effect becomes noticeable to stabilize the soil skeleton, resulting in an increase in the threshold dynamic stress amplitude.
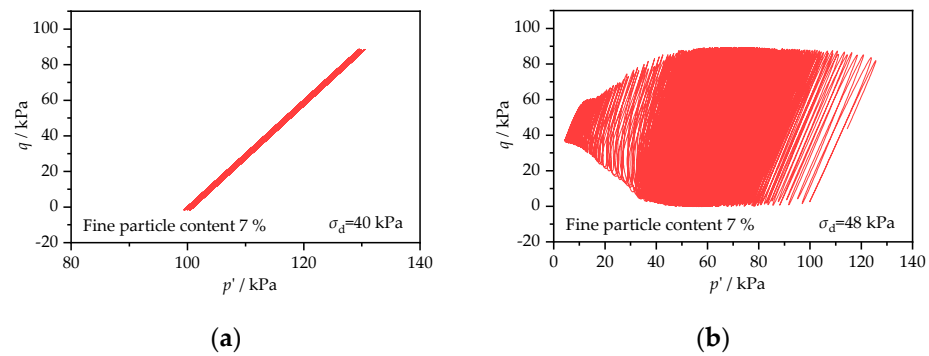
Figure 3. Stress path of the saturated silt with 7% fine particle content. (**a**) σ_d = 40 kPa (Stable mode); (**b**) σ_d = 48 kPa (Failure mode).
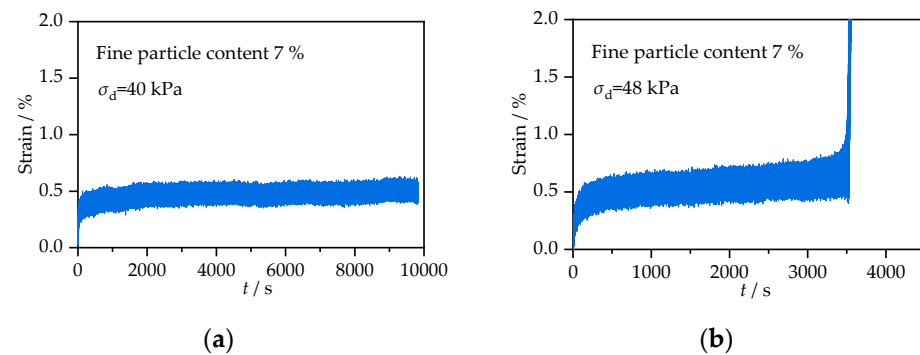

Figure 4. Accumulated strain of the saturated silt with 7% fine particle content. (**a**) σ_d = 40 kPa (Stable mode); (**b**) σ_d = 48 kPa (Failure mode).

Figure 5. Threshold dynamic stress amplitude and failure cycles of the silt with different fine particle contents.

Under undrained conditions, Figure 6 shows the excess pore water pressure (EPWP) versus the number of cycles of silt with different fine particle contents. The development of pore water pressure and permanent axial strain is similar and can be divided into two modes: stable mode and failure mode. When the cyclic stress is less than the threshold value, the excess pore water pressure rises quickly in the first few loading cycles before becoming stable as the number of cycles increases. When the cyclic stress exceeds the threshold value, the excess pore water pressure rises quickly in the early stages of vibration before slowing down. When the number of cycles approaches the failure cycles, however, the pore water pressure builds up quickly, causing the sample to be damaged. The accumulation rate of pore water pressure increases as the dynamic stress amplitude increases, and the soil sample reaches failure faster.
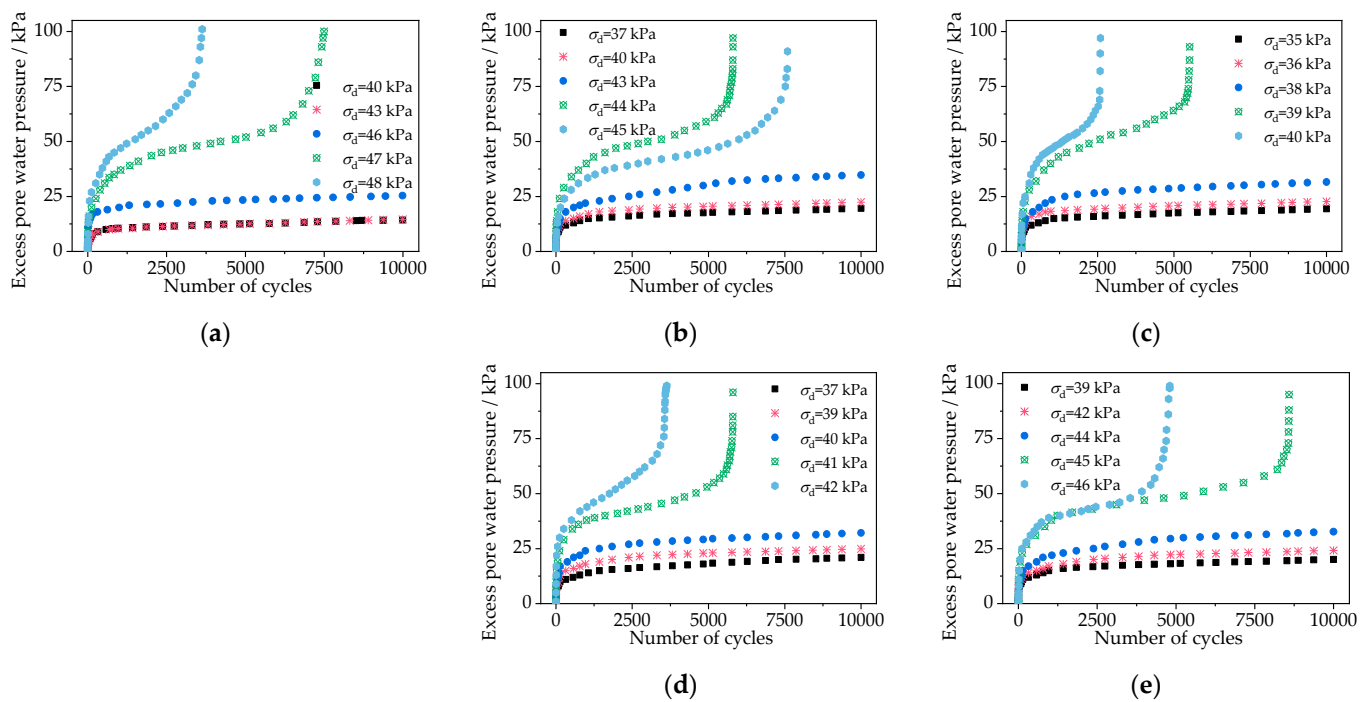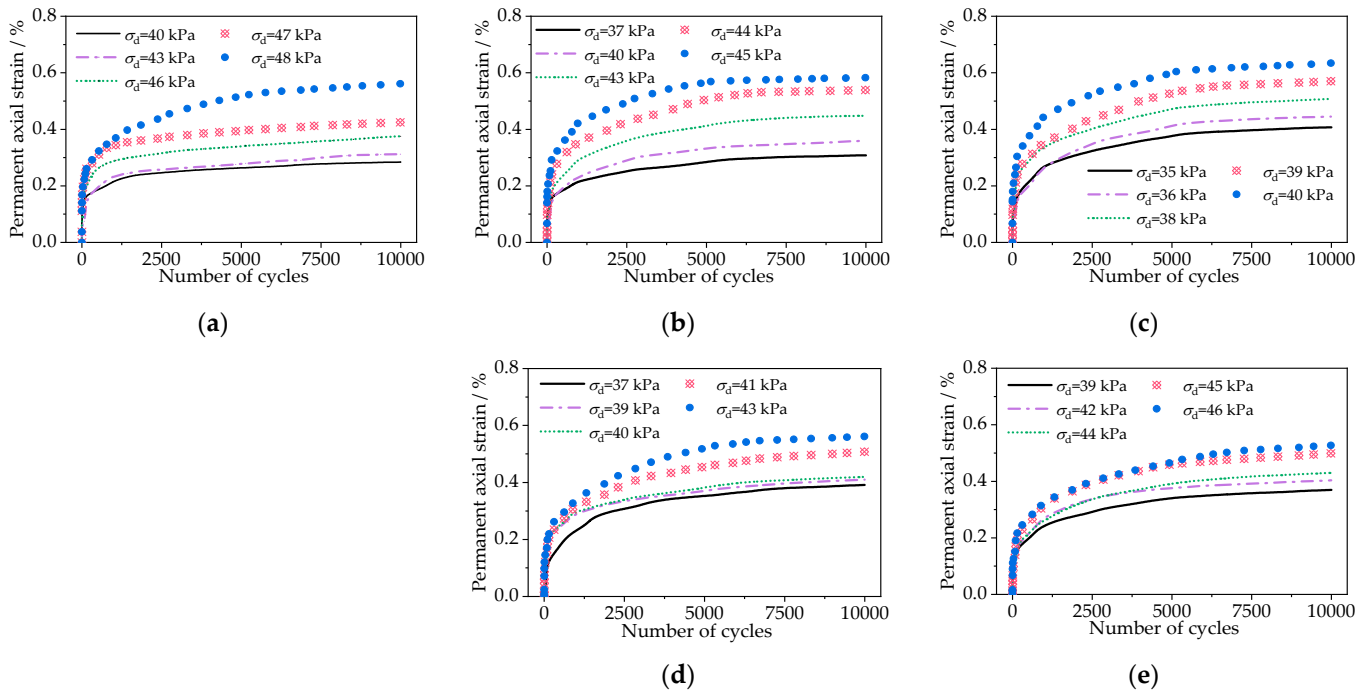
Figure 6. Excess pore water pressure of the saturated silt with different fine particle contents under undrained conditions. (**a**) 7% fine particle content; (**b**) 8% fine particle content; (**c**) 10% fine particle content; (**d**) 12% fine particle content; (**e**) 14% fine particle content.

3.2. Drained Cyclic Tests

Figure 7 depicts the permanent axial strain of the silt with different fine particle contents as a function of the number of cycles in drained conditions. Similar to the undrained condition, the strain increases rapidly under drained conditions at the beginning of cyclic loading and then tends to be stable. For some combinations of σ_d and fine particle content of the samples that fail under undrained conditions and respond in a stable mode under drained conditions, the permanent axial strain under drained conditions is smaller. The permanent axial strain increases as the dynamic stress amplitude increases, and the sample is not damaged within 10,000 cycles. Under the long-term train vibration of the metro line with the frequency near 1 Hz, a good drainage condition of the surrounding silt layer can effectively prevent deformation accumulation and liquefaction.

Figure 8 shows the relationship between the permanent axial strain at 10,000 cycles and the dynamic stress amplitude under different fine particle contents and drainage conditions, in which the dynamic stress amplitude that causes the failure of the sample (5% permanent strain) under undrained conditions is not considered. The permanent axial strain increases with the increase in dynamic stress amplitude. The growth rate of permanent axial strain is slow when the dynamic stress amplitude is small. The strain growth rate increases significantly in both drained and undrained conditions when the dynamic stress amplitude reaches the threshold value. The permanent axial strain is large at small dynamic stress amplitude when the fine particle content is 10%, indicating that silt's ability to resist cyclic loading is weakened. The permanent axial strain under drained conditions is greater than that under undrained conditions for the same fine particle content because the excess pore pressure is dissipated in time under drained conditions, which causes the consolidation deformation of the soil samples. At the same time, because the permeability of the sample is higher when the fine particle content is low, the difference between the undrained and drained permanent axial strain is more noticeable.

Figure 7. Permanent axial strain of the saturated silt with different fine particle contents under drained conditions. (**a**) 7% fine particle content; (**b**) 8% fine particle content; (**c**) 10% fine particle content; (**d**) 12% fine particle content; (**e**) 14% fine particle content.
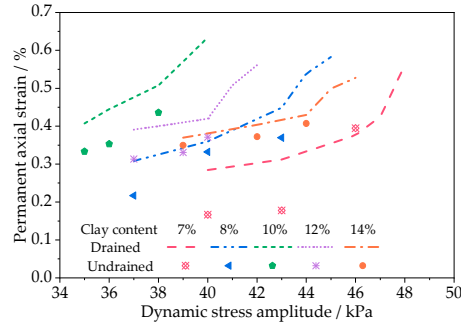

Figure 8. The relationship between permanent axial strain at 10,000 cycles and dynamic amplitude under different fine particle contents and drainage conditions.

4. Dynamic Response of the Silt Containing Fine Particles under Unloading Stress Paths

4.1. Pemanent Axial Strain under Different Unloading Intensities

The curves of permanent axial strain versus number of cycles of silt with 8% clay content for the unloading and unloading-reloading stress paths are shown in Figures 9 and 10, respectively. As shown in Figure 9, the silt produces accumulated tensile deformation and tensile failure along the unloading path at various unloading intensities. When the dynamic stress amplitude is less than the threshold value, the permanent strain rises quickly in the first few cycles before stabilizing. The permanent strain increases rapidly, and liquefaction failure occurs when the dynamic stress amplitude exceeds the threshold value and the number of cycles increases to the critical value. As shown in Figure 10, the unloading and reloading path accumulates compression strain, but the threshold dynamic stress amplitude decreases when compared to the conventional triaxial stress path (shown in Figure 2b), implying that the unloading and reloading process disturbs the soil sample.
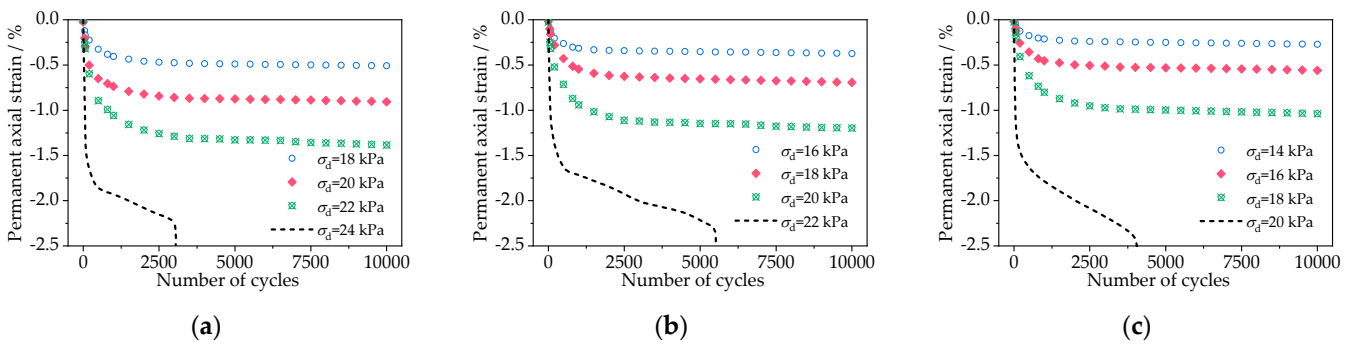
Figure 9. Permanent axial strain under unloading stress path. (**a**) BU−1 (unloading intensity = 10 kPa); (**b**) BU−2 (unloading intensity = 20 kPa); (**c**) BU−3 (unloading intensity = 40 kPa).
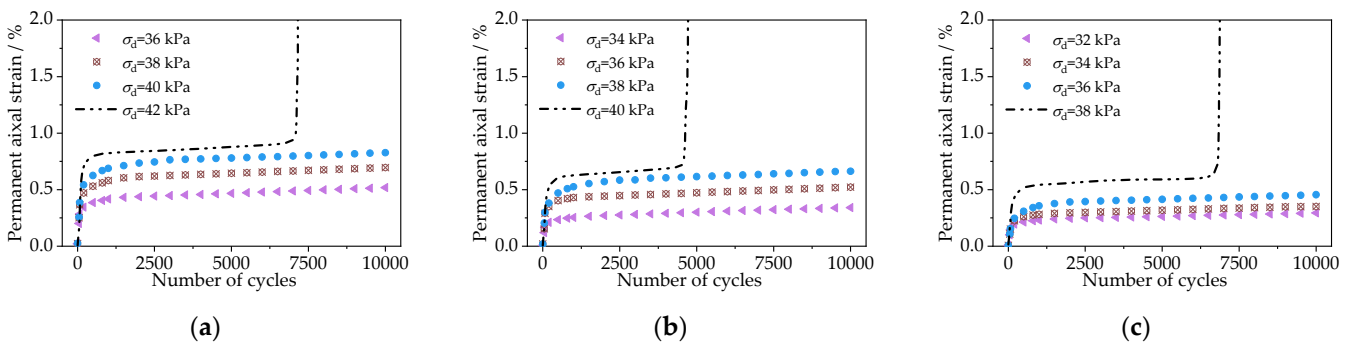
Figure 10. Permanent axial strain under unloading and reloading stress path. (**a**) CU−1 (unloading intensity = 10 kPa); (**b**) CU−2 (unloading intensity = 20 kPa); (**c**) CU−3 (unloading intensity = 40 kPa).

Under the unloading and unloading-reloading stress paths, Figure 11 shows the variation in threshold dynamic stress amplitude and failure cycles versus unloading intensities. Under a conventional triaxial path, the threshold dynamic stress amplitude and failure cycles of silt with 8% fine particle content are 44 kPa and 7577, respectively, according to Figure 5. Because the axial stress of the soil samples is reduced by 40 kPa under the unloading path, the threshold dynamic stress amplitude and failure cycles decrease significantly. The silt is disturbed during the unloading-reloading path, resulting in a small decrease in the threshold dynamic stress amplitude and failure cycles. The threshold dynamic stress amplitude of soil samples decreases slightly as the unloading intensity increases.
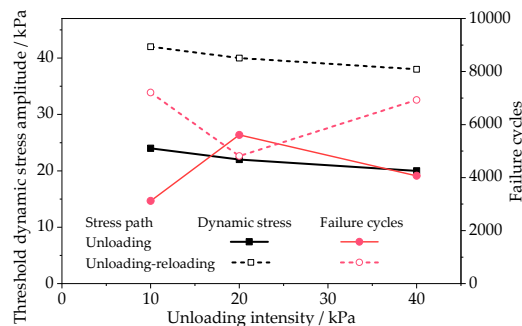

Figure 11. Threshold dynamic stress amplitude and failure cycles under different stress paths.
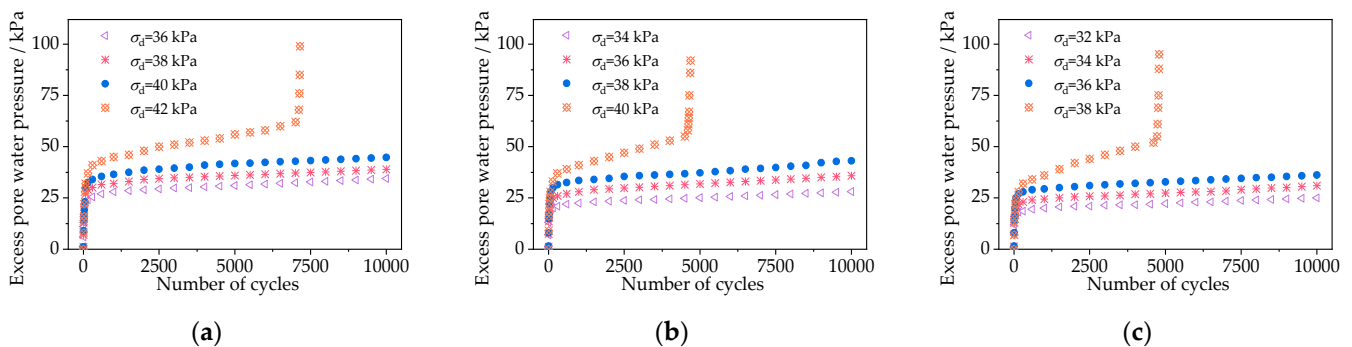
4.2. Excess Pore Water Pressure under Different Unloading Intensities

Excess pore water pressure of silt with 8% fine particle content under conventional triaxial, unloading, and unloading-reloading paths is shown in Figures 6b, 12 and 13. When the dynamic stress amplitude is less than the threshold value, the excess pore water pressure

rises quickly at first, then stabilizes as the number of cycles increases. The dynamic pore pressure rises rapidly to the confining pressure level when the dynamic stress amplitude exceeds the threshold value and the number of cycles is close to the critical value, resulting in liquefaction failure.
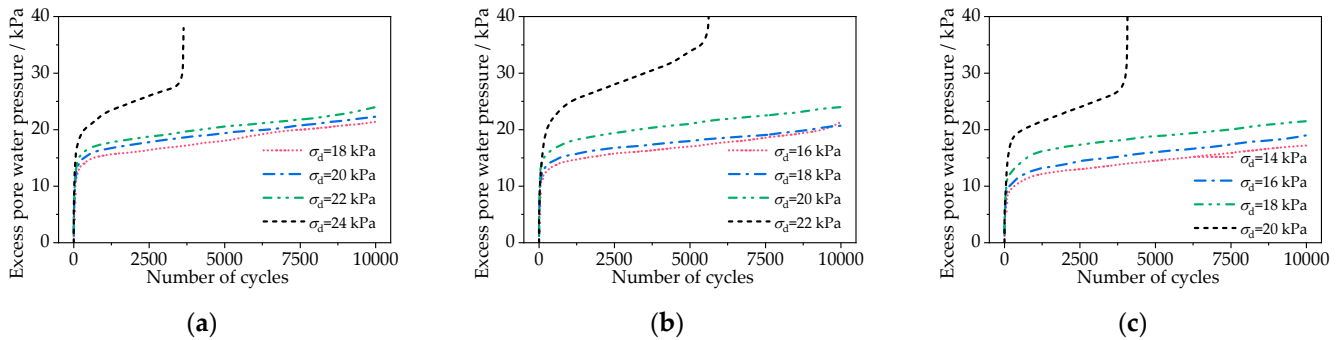
Figure 12. Excess pore water pressure under unloading stress path. (**a**) BU−1 (unloading intensity = 10 kPa); (**b**) BU−2 (unloading intensity = 20 kPa); (**c**) BU−3 (unloading intensity = 40 kPa).

Figure 13. Excess pore water pressure under unloading and reloading stress path. (**a**) CU−1 (unloading intensity = 10 kPa); (**b**) CU−2 (unloading intensity = 20 kPa); (**c**) CU−3 (unloading intensity = 40 kPa).

5. Conclusions

In order to evaluate the long-term deformation of the silt around the existing tunnel under the unloading of the above foundation pit and the cyclic loading of metro trains, a series of dynamic triaxial tests using the silt with different fine particle content and unloading intensities were carried out. The following conclusions are drawn:

1. In cyclic loading tests, there is a dynamic stress amplitude threshold. The permanent axial strain and excess pore water pressure of the silt tend to be stable as the number of cycles increases when the dynamic stress amplitude is less than this value. When the dynamic stress amplitude exceeds this value, the silt will liquefy and fail as the number of cycles increases. With increasing fine particle content, the threshold dynamic stress and failure cycles in silt decrease and then increase, reaching a minimum of 39 kPa and 5495, respectively, at 10% fine particle content.

2. For the same fine particle content, the permanent axial strain under drained conditions is greater than that under undrained conditions (when the sample does not fail at 10,000 cycles) because the excess pore pressure under drained conditions is dissipated in time, resulting in the consolidation deformation of soil samples. At the same time, due to higher permeability and lower fine particles of silt, the difference between undrained and drained permanent axial strain is more significant.

3. The threshold dynamic stress amplitude and failure cycles of the silt are significantly reduced by axial unloading. The silt is disturbed during the unloading and reloading path, resulting in a slight reduction in the critical dynamic stress amplitude and failure period. The dynamic stress threshold amplitude of a soil sample decreases slightly as unloading strength increases. As a result, the impact of fine particle content and foundation pit unloading on the dynamic characteristics of silt under long-term cyclic loading should be considered.

References

1. Tang, Y.; Cui, Z.; Zhang, X.; Zhao, S. Dynamic response and pore pressure model of the saturated soft clay around the tunnel under vibration loading of Shanghai subway. *Eng. Geol.* **2008**, *98*, 126–132. [CrossRef]
2. Xiao, J.; Juang, C.; Wei, K.; Xu, S. Effects of Principal Stress Rotation on the Cumulative Deformation of Normally Consolidated Soft Clay under Subway Traffic Loading. *J. Geotech. Geoenvironmental Eng.* **2014**, *140*, 4013046. [CrossRef]
3. Xia, C.; Meng, F.; Zhu, M.; Tang, Y.; Lu, C. Influence of Lateral Multistage Unloading Intensity on Mechanical Properties of Reconstituted Coastal Soils Containing Silty Particles. *Appl. Sci.* **2022**, *12*, 3651. [CrossRef]
4. Liu, J.; Xiao, J. Experimental Study on the Stability of Railroad Silt Subgrade with Increasing Train Speed. *J. Geotech. Geoenvironmental Eng.* **2010**, *136*, 833–841. [CrossRef]
5. Shen, Y.; Zhang, P.; Xu, G.; Liu, H. Dynamic strength characteristics and failure criteria of anisotropically consolidated silt under principal stress rotation. *J. Central South Univ.* **2013**, *20*, 2025–2033. [CrossRef]
6. Ng, C.; Zhou, C. Cyclic behaviour of an unsaturated silt at various suctions and temperatures. *Geotechnique* **2014**, *64*, 709–720. [CrossRef]
7. Juneja, A.; Mohammed-Aslam, A. Post-cyclic undrained response of sand and silt. *Soil Dyn. Earthq. Eng.* **2020**, *133*, 106138. [CrossRef]
8. Cui, X.; Zhang, N.; Zhang, J.; Gao, Z. In situ tests simulating traffic-load-induced settlement of alluvial silt subsoil. *Soil Dyn. Earthq. Eng.* **2014**, *58*, 10–20. [CrossRef]
9. Georgiannou, V.; Hight, D.; Burland, J. Behaviour of clayey sands under undrained cyclic triaxial loading. *Geotechnique* **1991**, *41*, 383–393. [CrossRef]
10. Ansal, A.; Erken, A. Undrained Behavior of Clay Under Cyclic Shear Stresses. *J. Geotech. Eng. ASCE* **1989**, *115*, 968–983. [CrossRef]
11. Mamou, A.; Powrie, W.; Priest, J.; Clayton, C. The effects of drainage on the behaviour of railway track foundation materials during cyclic loading. *Geotechnique* **2017**, *67*, 845–854. [CrossRef]
12. Cavallaro, A.; Capilleri, P.; Grasso, S. Site Characterization by Dynamic In Situ and Laboratory Tests for Liquefaction Potential Evaluation during Emilia Romagna Earthquake. *Geosciences* **2018**, *8*, 242. [CrossRef]
13. Dash, H.; Sitharam, T.; Baudet, B. Influence of Non-Plastic Fines on the Response of a Silty Sand to Cyclic Loading. *Soils Found.* **2010**, *50*, 695–704. [CrossRef]
14. Akhila, M.; Rangaswamy, K.; Sankar, N. Undrained Response and Liquefaction Resistance of Sand–Silt Mixtures. *Geotech. Geol. Eng.* **2018**, *37*, 2729–2745. [CrossRef]
15. Ghani, S.; Kumari, S. Insight into the Effect of Fine Content on Liquefaction Behavior of Soil. *Geotech. Geol. Eng.* **2020**, *39*, 1–12. [CrossRef]

16. Qian, J.; Du, Z.; Lu, X.; Gu, X.; Huang, M. Effects of principal stress rotation on stress–strain behaviors of saturated clay under traffic–load–induced stress path. *Soils Found.* **2018**, *59*, 41–55. [CrossRef]

17. Triantafyllos, P.; Georgiannou, V.; Dafalias, Y.; Georgopoulos, I. Novel findings on the dilatancy and non-coaxiality of sand under generalised loading. *Acta Geotech.* **2020**, *16*, 1699–1734. [CrossRef]

18. Indraratna, B.; Korkitsuntornsan, W.; Nguyen, T. Influence of Kaolin content on the cyclic loading response of railway subgrade. *Transp. Geotech.* **2020**, *22*, 100319. [CrossRef]

19. Shen, S.; Wu, H.; Cui, Y.; Yin, Z. Long-term settlement behaviour of metro tunnels in the soft deposits of Shanghai. *Tunn. Undergr. Space Technol.* **2014**, *40*, 309–323. [CrossRef]

20. Zhu, M.; Gong, X.; Gao, X.; Liu, S.; Yan, J. Remediation of Damaged Shield Tunnel Using Grouting Technique: Serviceability Improvements and Prevention of Potential Risks. *J. Perform. Constr. Facil.* **2019**, *33*, 4019062. [CrossRef]

21. Liu, Z.; Xue, J.; Yaghoubi, M. The effects of unloading on undrained deformation of a kaolin clay under cyclic loading. *Soil Dyn. Earthq. Eng.* **2020**, *140*, 106434. [CrossRef]

22. Liu, Z.; Xue, J.; Mei, G. The impact of stress disturbance on undrained cyclic behaviour of a kaolin clay and settlement of tunnels under cyclic loading. *Acta Geotech.* **2021**, *16*, 3947–3961. [CrossRef]

23. Ding, Z.; Zhang, T.; Wei, X.; Zhang, M. Experimental study on the cyclic loading of metro trains. *Chin. Earthq. Eng. J.* **2015**, *37*, 789–793.

24. Gong, Q.; Xu, Y.; Zhou, S. Dynamic response analysis of tunnel foundation by vehicle vibration in metro. *Chin. Railw. Sci.* **2005**, *26*, 47–51.

25. Seed, H.; Idriss, I.; Arango, I. Evaluation of Liquefaction Potential Using Field Performance Data. *J. Geotech. Eng.* **1983**, *109*, 458–482. [CrossRef]